Available online at www.sciencedirect.com
SCIENCE DIRECT®
PERGAMON
International Journal of Heat and Mass Transfer 46 (2003) 2389–2402
International Journal of HEAT and MASS TRANSFER
www.elsevier.com/locate/ijhmt

Natural convection from narrow horizontal plates at moderate Rayleigh numbers

Ingrid Martorell [a], Joan Herrero [a], Francesc X. Grau [b,*]

[a] Departament d'Enginyeria Química, Universitat Rovira i Virgili, Campus Sescelades, Avda Països Catalans 26, 43007 Tarragona, Catalunya, Spain

[b] Departament d'Enginyeria Mecànica, Universitat Rovira i Virgili, Campus Sescelades, Avda Països Catalans 26, 43007 Tarragona, Catalunya, Spain

Received 6 August 2001; received in revised form 21 November 2002

Abstract

The present work deals with the natural convection flow and heat transfer from a horizontal plate cooled from above. Experiments are carried out for rectangular plates having aspect ratios between $\phi = 0.036$ and 0.43 and Rayleigh numbers in the range $290 \leqslant Ra_w \leqslant 3.3 \times 10^5$. These values of Ra_w and ϕ have been selected below those commonly considered in previous research in view of a future application to the design of printed circuit boards. The plates are made of two different metals, copper and steel. The choice of a metal is relevant to the present problem because the plates are heated by means of an electric current. Important variations of the surface temperature are observed along the transverse direction for the steel plates. The surface of the copper plates is almost isothermal because of the high thermal conductivity of the metal.

Calculations for a semi-infinite plate are carried out to predict the transverse profiles of the surface temperature and heat flux and to visualize the structure of the flow. Three-dimensional calculations are also used at a qualitative level to observe the changes in the flow structure due to the finite length of the plate. Present results are compared with both previous experimental work and analyses that are based on boundary layer theory. It is shown that analyses for an infinite boundary layer are not completely applicable to the present problem because of its different physics. The most relevant feature of the natural convection flow, which is not predicted by boundary layer analyses, is a thermal plume rising near the center of the plate.

Present heat transfer results differ from previous experimental work because of the lower Rayleigh numbers and aspect ratios investigated here. The Nusselt number is found to depend on Ra_w^n, with the exponent $n = 0.17$ being lower than most of the values reported in the literature. This comparatively low value is related to the transverse conduction of heat through the air, which becomes increasingly significant as Ra_w approaches zero. It is shown that such a low-Ra_w effect can be accounted for in a physically consistent manner by adding a constant term to the heat transfer correlation. On the other hand, it is found that the Nusselt number does not significantly depend on the aspect ratio in the range of ϕ investigated contrary to what has been previously reported for wider plates.

Keywords: Heat transfer; Natural convection; Plate

1. Introduction

Applications of natural convection to the cooling of electronic equipment have received much attention in the last decades because of its practical interest [1]. The present investigation was originated during the development of a calculation tool for the prediction of the

* Corresponding author. Tel.: +34-977-559640; fax: +34-977-559691.
E-mail address: xgrau@etseq.urv.es (F.X. Grau).

0017-9310/03/$ - see front matter © 2003 Elsevier Science Ltd. All rights reserved.
doi:10.1016/S0017-9310(03)00010-3

Nomenclature

A	surface area, m^2
f	function
g	acceleration of gravity, m/s^2
h	heat transfer coefficient, $W/m^2\,K$, defined in Eq. (4)
I	intensity, A
k	thermal conductivity, W/m K
L	length of the plate, m
ℓ	characteristic length in Eqs. (5) and (6), m
m	exponent used in the heat transfer correlations; see Eq. (13)
Nu	Nusselt number, Eq. (5)
p	pressure, Pa
P	perimeter of the plate, m
Pr	Prandtl number
q	heat transfer rate, W
q''	heat flux, W/m^2
Ra^*	modified Rayleigh number, Eq. (10)
Ra	Rayleigh number, Eq. (6)
t	time, s
T	temperature, K
U_y	velocity in the y-direction, m/s
U_z	velocity in the z-direction, m/s
W	width of the plate, m
x	coordinate across the plate length, m
y	coordinate across the plate width, m
Δy	minimum grid spacing along the y-direction used in 2D calculations, m
z	height coordinate, m
Δz	minimum grid spacing along the z-direction used in 2D calculations, m
ΔT	$\Delta T = \overline{T}_s - T_\infty$, K
$\Delta_x T_s$	longitudinal temperature drop along the surface of the plate, K

Greek symbols

α	thermal diffusivity, m^2/s
β	thermal expansion coefficient, K^{-1}
Γ	$\Gamma = 1/(2(1+\phi)) = \eta/W$
δ	thickness of the plate, m
Δ	variation
ε	emissivity of the surface
ϕ	aspect ratio of the plate, $\phi = W/L$
γ	exponent used in Eq. (7)
θ	dimensionless temperature, $\theta = (T_{max} - T)/(T_{max} - T_\infty)$
η	$\eta = A/P$, m
ρ	density, kg/m^3
ν	kinematic viscosity, m^2/s
σ	Stefan–Boltzmann constant

Subscripts

cond	conduction
conv	convection
dis	dissipation
max	maximum
met	metal
rad	radiation
∞	ambient room conditions
s	surface of the plate
w	based on the plate width
η	based on the area to perimeter ratio, η

Superscript

–	average

heat transfer from printed circuit boards (PCB's) used in the automotive industry [2]. These PCB's incorporate a large number of electronic components connected by a network of metal tracks that transport the electric charge. Although the electronic components are usually the source of most of the heat generated in the PCB, the heating of the tracks by dissipation of electric charge is by no means negligible. Moreover, part of the heat generated in the electronic components is transferred to the tracks nearby. The cooling of the tracks, which in the worst case is caused by natural convection alone, is therefore a key factor in the performance of the equipment. Even with the help of today's powerful computers, a detailed calculation of the three-dimensional (3D) flow and heat transfer problem, which is in addition coupled with the electric field, is still very challenging. Thus, an approximate evaluation of the heat transfer coefficients by means of empirical correlations is still to be preferred in the design of PCB's, at least at the preliminary level.

Before dealing with the more complex shapes typically encountered in PCB's, it was decided to investigate the problem of an upward facing warm rectangular plate. A literature survey on natural convection from horizontal plates [3–15] convinced the authors that this problem, despite its apparent simplicity, is not fully characterized yet. In particular, two aspects deserve a more detailed investigation. First, the possible dependence of the Nusselt number on the aspect ratio, $\phi = W/L$, for narrow plates, e.g., plates having aspect ratios below $\phi = 0.10$. Second, the characterization of the heat transfer rates within a range of Rayleigh numbers of practical interest to the PCB design problem, namely $10^2 \leqslant Ra_w \leqslant 10^6$. These two points are further discussed in relation to the previous research in the field.

In the $\phi \to 0$ limit, that is, very long or very narrow plates, the natural convection flow above the plate should be two-dimensional (2D). This flow consists of a

thermal plume upwelling at the center of the plate with air being transported from the edges within two mirror-symmetric boundary layers [12,15,16]. However, for plates having a finite length the flow is 3D near the two ends of the plate. This might result in a dependence of the Nusselt number on the aspect ratio of the plate [15]. Such dependence is obviated in much of the previous work where the behavior of a semi-infinite plate is assumed [3,5,6,9–13]. Fig. 1a shows the equations proposed by several authors for the dependence of the Nusselt number on the Rayleigh number when these dimensionless groups are based solely on the width of the plate. Note that correlations in Fig. 1a exhibit different slopes in the logarithmic plot, e.g., different values of the exponent in the Ra_w^n term. Several of the equations plotted in Fig. 1a agree fairly well in the range of Rayleigh numbers they are devised for, typically $10^6 \leqslant Ra_w \leqslant 10^7$. However, dispersion grows dramatically as the Rayleigh number decreases. For example, at $Ra_w = 10^3$ predictions for the Nusselt number range between $Nu_w \approx 1$ and 5. Thus, the correlations plotted in Fig. 1a may be inapplicable to the range of Rayleigh numbers that is relevant to the present investigation.

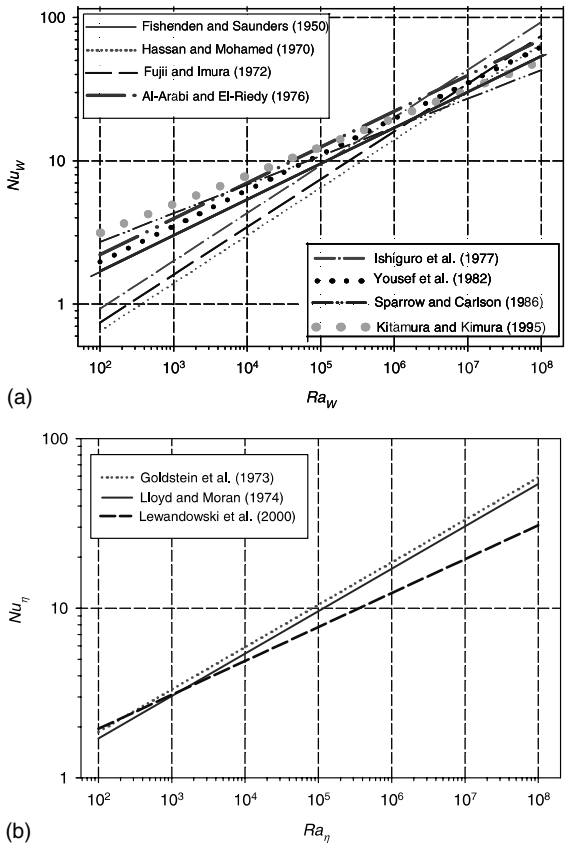

Fig. 1. Published heat and mass transfer correlations for natural convection from horizontal plates. The plate width, W, is used as the characteristic length in (a) while the correlations in (b) use the area over perimeter ratio, η.

Other authors [7,8,15] define Rayleigh and Nusselt numbers that are based on the area to perimeter ratio, η, to account for the dependence of Nu on the geometry of the plate. Heat transfer correlations of this second type obtained for aspect ratios higher than $\phi = 0.20$ are shown in Fig. 1b. The problem with the correlations plotted in Fig. 1b is that, as shown in Section 3.2 below, equations based on the hydraulic radius, η, may not be applicable to plates having a low ϕ.

The effect of the plate geometry on the Nusselt number is assessed in the present work by means of experiments performed for aspect ratios in the range $0.036 \leqslant \phi \leqslant 0.43$. The plates are made of metal, either copper or steel, and are heated by means of a continuous electric current. While important transverse temperature variations are expected for the steel plates [12], the copper plates should yield almost uniform temperature distributions because of the much higher thermal conductivity of the metal. Comparison of results for the two types of plates will therefore show whether the presence of a transverse temperature drop has an effect on the structure of the flow and the rate of heat transferred from the surface.

On the other hand, 2D and 3D calculations are also performed. Two-dimensional calculations incorporate a special treatment for the surface of the plate that assumes a uniform heat generation per unit volume within the metal. This treatment, more realistic than the assumption of either a uniform temperature or a uniform heat flux, allows the characterization of the transverse profiles of these two quantities at the plate surface. Calculations also provide a picture of the natural convection flow and allow establishing comparisons between predictions and both present measurements and previous theory.

The remainder of the paper is organized as follows. The experimental setup and techniques used are presented in Section 2. The different analytical and calculation methods employed to obtain and analyze current results are discussed in Section 3. The results of the present investigation are presented and discussed in Section 4. Finally, conclusions are drawn in Section 5.

2. Experimental apparatus and procedures

Thirty-five μm thick copper plates and 50 μm thick steel plates are used in the experiments. Each plate features a rectangular test area of length L and width W in contact with air. The aspect ratio of the plates, $\phi = W/L$, ranges between $\phi = 0.036$ and 0.43, as listed in Table 1. The bottom face of the plates is attached to a 1.5 mm thick layer of fiberglass, as shown in Fig. 2a. In turn, the fiberglass layer is supported on a 3.0 cm thick

Table 1
Summary of the plate dimensions used in the present experiments

Metal	L (cm)	W (cm)	$\phi = W/L$
Copper	28.0	1.0	0.036
Copper	23.0	1.0	0.043
Copper	14.0	1.0	0.071
Copper	23.0	2.0	0.087
Copper	28.0	2.5	0.089
Copper	23.0	2.5	0.109
Stainless steel	23.0	2.5	0.109
Stainless steel	23.0	3.0	0.130
Copper	14.0	2.0	0.143
Copper	23.0	4.0	0.174
Stainless steel	23.0	4.0	0.174
Copper	14.0	2.5	0.179
Copper	28.0	5.0	0.179
Stainless steel	23.0	5.0	0.217
Copper	23.0	6.0	0.261
Copper	25.4	7.62	0.300
Copper	23.0	9.0	0.391
Copper	14.0	6.0	0.429

block of extruded polystyrene (Glascofoam-DOW, $k = 0.052$ W/m K); see Fig. 2b. The plate and insulation block ensemble is embedded in a topless Plexiglas box 34 cm × 12 cm × 5 cm (x, y, z).

The two plate ends, where cables and connectors are jointed, are bent 45° downwards and covered by the two sliding lids. This setup allows air to enter the region above the test area both from the sides and longitudinally, e.g., traveling above the two sliding lids. Thus, a 3D-flow structure should be expected near the plate ends. Moreover, in order to rule out undesired effects that would complicate the physics of the problem, the longitudinal temperature drop along the surface of the plate, $\Delta_x T_s$, is checked during the experiments. This temperature drop is very low for the copper plates, namely $\Delta_x T_s \leqslant 0.01\Delta T$, and comparatively higher for the steel plates because of the lower thermal conductivity of the metal. Here, ΔT is the difference between the average temperature of the plate surface and the ambient air temperature. Notwithstanding, in the latter case the longitudinal variation of temperature remains below $\Delta_x T_s \leqslant 0.05\Delta T$ for moderate values of ΔT.

The experimental apparatus is mounted on a perfectly horizontal table. A much bigger bottomless 84 cm × 70 cm × 50 cm Plexiglas box is placed on the table so that it symmetrically surrounds the experimental apparatus and a big volume of air around it. This arrangement ensures that no external disturbances in the room air interfere with the experiments. It has been verified that experimental results can be reproduced in the absence of the big box if the air in the room remains undisturbed. The plates are heated by means of a continuous electric current provided by an analog programmable power supply (HP-6541A, 0–8 V/0–20 A). The room ambient temperature is controlled by a heat-pump system. Temperatures are measured using type-K thermocouples that are monitored in a data acquisition unit (HP-34970A) that is in turn connected to a personal computer. Heat losses through the bottom fiberglass layer are measured using episensors (Vatell

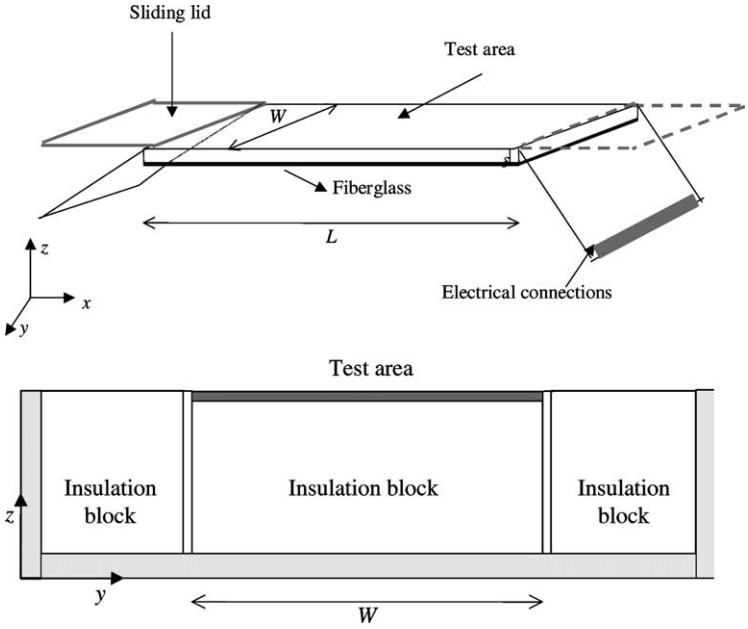

Fig. 2. Sketch of the experimental setup used in the present investigation.

Corporation). The primary output from the episensor is a heat flux measurement that is obtained from a thermopile heat flux sensor with high sensitivity and a low thermal resistance that occupies most of the surface area on the sensor face. The sensor acts like a differential voltage source with the value of the voltage being proportional to the heat flux and its time of response is below 6 μs.

Thermochromic liquid crystals (TLC's) are used to check the thermocouple readings and, especially, to measure the transversal temperature profiles which show, in the case of the steel plates, important variations of T_s. Microencapsulated chiral-nematic TLC's (manufactured by Hallcrest LC Technology) with a narrow band of approximately 5 K are employed to measure temperature between 293 and 313 K. The accessory equipment consists of a calibration unit, a RGB video camera (Sony DXC-151) connected to a personal computer, a 250 W white light focus and the corresponding software [17]. The emissivities of the copper and TLC surfaces are measured with the help of a reference black surface of known emissivity and a radiometer. Emissivity values of $\varepsilon = 0.174 \pm 0.004$, $\varepsilon = 0.902 \pm 0.008$ have been measured for the copper and TLC surfaces, respectively. The steel plates are always coated with a TLC layer in order to measure the surface temperature, which, as mentioned above, features important variations in the y-direction.

3. Analysis and data reduction

3.1. Energy balance

The steady-state energy balance for a heated plate may be written as:

$$q_{conv} = q_{dis} - q_{rad} - q_{cond} \tag{1}$$

In order to evaluate q_{conv}, the rate of heat transferred from the plate surface into the air, it is therefore necessary to evaluate each of the terms in the right-hand-side (RHS) of Eq. (1). The physical properties of air are evaluated at the film temperature. The heat generated by Joule effect is obtained from the measured potential drop. The uniformity of the voltage drop per unit of longitudinal distance, $\Delta V/\Delta x$, along the transversal position, y, is evidenced by measurements. The rate of heat dissipation is therefore calculated as:

$$q_{dis} = \Delta V I \tag{2}$$

The heat radiation term is estimated from the Stefan–Boltzmann law. The radiation heat exchange between the plate surface and its surroundings is evaluated according to:

$$q''_{rad} = \sigma\varepsilon\left(T_s^4 - T_\infty^4\right) \tag{3}$$

In the experiments with steel plates, where important variations of the surface temperature are observed, the heat radiation term, q_{rad}, is obtained by integration along the y-direction of the local heat flux values given by Eq. (3). The heat losses by conduction through the bottom of the plate are measured, as discussed above, using episensors. Unfortunately, the smallest episensors available are 2.5 cm wide so that an indirect method has to be used for narrower plates. It has been checked that the q_{cond} values measured from plates with $W \geqslant 2.5$ cm are satisfactorily predicted by solving the heat conduction equations within the insulation block. This approach, which also includes the use of measured temperature values to characterize the boundary conditions, is used to evaluate the q_{cond} term for the narrower plates.

3.2. Correlation of heat transfer data

The values of the convection heat fluxes obtained from Eq. (1) are used to evaluate the corresponding average heat transfer coefficients,

$$\bar{h} = \frac{q_{conv}}{A\,\Delta\overline{T}} \tag{4}$$

Non-dimensional groups relevant to the characterization of the heat transfer coefficient are the Nusselt number, Nu, the Rayleigh number, Ra, and the Prandtl number, Pr. Both Ra and Nu are based on a characteristic length of the problem, ℓ,

$$Nu = \frac{\bar{h}\ell}{k} \tag{5}$$

$$Ra = \left(\frac{g\beta}{\nu^2}\right)\Delta T \ell^3 Pr = \left(\frac{g\beta}{\alpha\nu}\right)\Delta T \ell^3 \tag{6}$$

The relation between the three dimensionless groups, Ra, Nu and Pr, is generally given in the form:

$$Nu = CRa^n Pr^\gamma \tag{7}$$

The dependence of the Nusselt number on the Prandtl number will be dropped hereinafter since air is the only fluid of interest in the present investigation. The boundary layer analysis of natural convection from a horizontal surface [18] suggests a value of $\gamma = 0.05$ in Eq. (7) thus yielding variations in the Pr^γ term between 0.89 for $Pr = 0.10$ and 1.12 for $Pr = 10$. A more complex dependence of Nu on Pr is given in Ref. [6].

As discussed above, the length definitions commonly used in Eqs. (5) and (6) are the width of the plate, $\ell = W$, and the area to perimeter ratio, $\ell = \eta$. The latter length is used, among other authors [7,8], by Lewandowski et al. [15] who have recently proposed the following correlation:

$$Nu_\eta = 0.774 Ra_\eta^{0.20} \quad 5 \times 10^4 \leqslant Ra_\eta \leqslant 5 \times 10^6; \;\; 0.21 \leqslant \phi \leqslant 1 \tag{8}$$

Among the published heat transfer correlations based on the plate width [3,5,6,9–14], the most frequently referenced is probably the one provided by Sparrow and Carlson [12], which can be written as,

$$Nu_w = CRa_w^n \tag{9}$$

with $C = 1.08$ and $n = 1/5$. It must be pointed out that Sparrow and Carlson [12] actually use a modified Rayleigh number defined as,

$$Ra^* = \frac{g\beta}{\alpha\nu k} q''_{conv} W^4 \tag{10}$$

and that their original correlation is given in the form,

$$Nu_w = 1.07(Ra^*)^{1/6} \quad 2.7 \times 10^6 \leqslant Ra^* \leqslant 2.3 \times 10^7 \tag{11}$$

It is easy to see that Eqs. (5), (6) and (11) can be combined to obtain Eq. (9). In order to unify the treatment for semi-infinite and finite plates, equations based on η may be written in a different manner:

$$\eta = \frac{LW}{2(L+W)} = W\frac{L}{2(L+W)} = W\left(\frac{1}{2(1+\phi)}\right)$$
$$\Rightarrow Nu_\eta = Nu_w\Gamma; \quad Ra_\eta = Ra_w\Gamma^3 \tag{12}$$

$$Nu_w = CRa_w^n\Gamma^{3n-1} = CRa_w^n\Gamma^m \tag{13}$$

$$Nu_w = Cf(\phi)Ra_w^n \tag{14}$$

It is worth to note that the form of Eq. (14) may also be inferred from a dimensional analysis. Comparison of the last two equations suggests that the condition $f(\phi) = \Gamma^m = \Gamma^{3n-1}$ in Eq. (13) is a constraint arising from the choice of η as the characteristic length in Eqs. (5) and (6). The more general form of Eq. (14) illustrates better than Eq. (13) the idea behind the use of a geometrical parameter in heat transfer correlations. As ϕ increases, the term $f(\phi)$ should play a progressively more important role in Eq. (14). As an example, in the correlation of Lewandowski et al. [15], Eq. (8), the geometry function ranges between $Cf(\phi) = 1.11$ for $\phi = 0.215$ and $Cf(\phi) = 1.35$ for $\phi = 1$. Correlations that are solely based on the plate width, e.g., Eq. (9) above, can be understood as a particular case of Eq. (14) in the limit of $f(\phi) \to 1$ as $\phi \to 0$.

The form commonly used to correlate heat transfer data [4,7,8,15] is not Eq. (14) but rather that of Eq. (8) e.g., $Nu_\eta = CRa_\eta^n$. If Eq. (13) is written as,

$$(Nu_w\Gamma) = Nu_\eta = CRa_\eta^n = C\left(Ra_w^n\Gamma^{3n}\right) \tag{15}$$

it becomes clear that a plot of Nu_η vs. Ra_η stresses the influence of the geometry since both the ordinate and the abscissa are a function of Γ. The inconvenient of Eq. (15) when fitting data by least squares is that the statistical weight of the n exponent is diminished. This point is illustrated by the simple numerical experiment that is discussed in what follows. The data points shown in Fig. 3 are generated numerically by first assuming a set of Ra_w values uniformly distributed within a range similar to that observed in the present experiments. The values of Nu_w are then computed according to Sparrow and Carlson's correlation [12], e.g., Eq. (9) with $C = 1.08$ and $n = 1/5$. Note that this procedure generates values of Nu_w that do not depend on the aspect ratio. The corresponding values of Ra_η and Nu_η are computed by assigning values of Γ in the range $0.30 \leqslant \Gamma \leqslant 0.50$ $(0 \leqslant \phi \leqslant 2/3)$, as indicated by the symbols in the plots. The imposed presence of the aspect ratio in Fig. 3 falsifies the dependence of Nu_w on Ra_w. The best fit to data in Fig. 3 is $Nu_\eta = 1.054Ra_\eta^{0.152}$. Although this equation can be used to obtain predictions of Nu_w within $\pm 5\%$ of the original synthetic values, the exponent $n = 0.152$ is remarkably lower than the original $n = 1/5$.

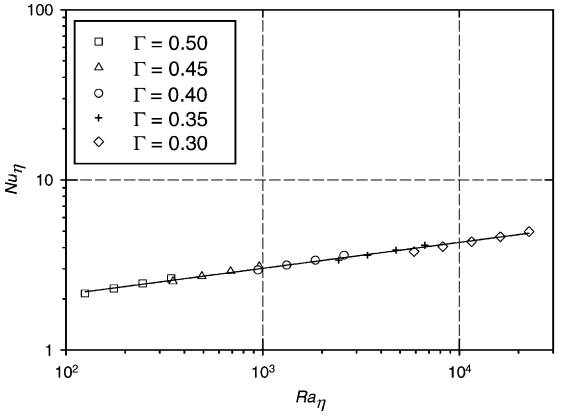

Fig. 3. Plot of synthetic heat transfer data generated according to Eq. (9) with $C = 1.08$ and $n = 1/5$. A value of the geometrical parameter Γ is associated to each data point as indicated by the symbols.

Obviously, a multi-linear regression analysis of the numerical data based on Eq. (14) with $f(\phi) = \Gamma^m$ or $f(\phi) = \phi^m$ yields $m = 0$ so that the original $C = 1.08$ and $n = 1/5$ constants are perfectly recovered. The use of Eq. (15) in Fig. 3 induces however a false dependence of Nu_w on $\Gamma^{-0.54}$. Thus, even though Eq. (9) would appear as a particular case of Eq. (15) for $\phi \to 0$, the latter equation cannot be safely applied when Nu_w does not actually depend on the area to perimeter ratio, η. The more solid Eq. (14) is therefore used to analyze the present heat transfer data.

3.3. Calculations

Two-dimensional calculations of the natural convection flow and heat transfer are performed using the computing unsteady three-dimensional elliptic flows (CUTEFLOWS) numerical algorithm [19]. The code

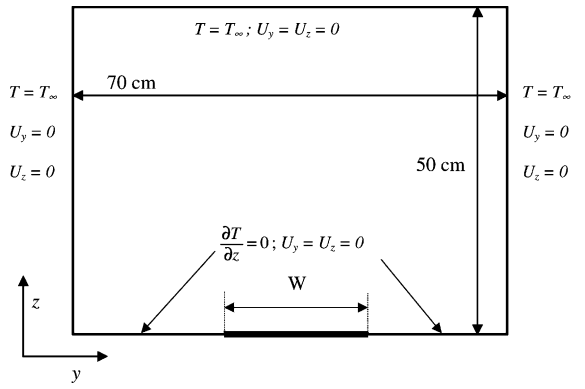

Fig. 4. Schematic of the geometry and boundary conditions prescribed in the 2D calculations of the natural convection flow over a semi-infinite plate of width W. Note that the drawing is not to scale.

solves a discrete form of the differential conservation equations of mass, momentum and energy. These equations may be written, in the context of Fig. 4, as:

mass:

$$\frac{\partial U_y}{\partial y}+\frac{\partial U_z}{\partial z}=0 \tag{16}$$

y-momentum:

$$\rho_\infty\left(\frac{\partial U_y}{\partial t}+\frac{\partial U_y^2}{\partial y}+\frac{\partial U_z U_y}{\partial z}\right) = -\frac{\partial p}{\partial y}+\mu\left(\frac{\partial^2 U_y}{\partial y^2}+\frac{\partial^2 U_y}{\partial z^2}\right) \tag{17}$$

z-momentum:

$$\rho_\infty\left(\frac{\partial U_z}{\partial t}+\frac{\partial U_y U_z}{\partial y}+\frac{\partial U_z^2}{\partial z}\right) = -\frac{\partial(p+\rho_\infty gz)}{\partial z}+\rho_\infty g\beta(T-T_\infty)+\mu\left(\frac{\partial^2 U_z}{\partial y^2}+\frac{\partial^2 U_z}{\partial z^2}\right) \tag{18}$$

energy:

$$\frac{\partial T}{\partial t}+\frac{\partial U_y T}{\partial y}+\frac{\partial U_z T}{\partial z}=\alpha\left(\frac{\partial^2 T}{\partial y^2}+\frac{\partial^2 T}{\partial z^2}\right) \tag{19}$$

Note that the effect of buoyancy is introduced in Eq. (18) by means of the Boussinesq assumption. The calculation algorithm solves the discrete form of Eqs. (16)–(19) by means of a second-order accurate finite-volume scheme (details of the algorithm may be found in Ref. [19]). The code has been successfully benchmarked and used in calculations of either isothermal flows and natural and mixed convection flows; see Ref. [20] and the references therein.

The dimensions of the 2D-calculation domain, sketched in Fig. 4, match those in the experimental setup, e.g., the side and height of the urn, 70.0 cm in the y-direction and 50.0 cm in the z-direction. Boundary conditions prescribed at the plate surface are more realistic than either the uniform temperature or the uniform heat flux condition. In the context of Figs. 1 and 4, the energy balance (1) is locally imposed within each calculation cell at the surface boundary, that is,

$$k_\infty \left.\frac{\partial T}{\partial z}\right|_s = q''_{\rm dis}-\sigma\varepsilon(T_s^4-T_\infty^4)-\left.q''_{\rm cond}\right|_z-\frac{k_{\rm met}\delta}{\Delta y}\frac{\partial T_s}{\partial y}s \tag{20}$$

where Δy is the width of the calculation cell, δ is the thickness of the metal plate and $k_{\rm met}$ is its thermal conductivity. The values of the vertical conduction losses, the third term on the RHS of Eq. (20), and the heat generated per unit surface, $q''_{\rm dis}$, are taken from measurements. The most relevant feature in Eq. (20) is in the last term of the RHS, which accounts for the transversal conduction of heat within the metal plate. At each time step, the discrete form of Eq. (20) is solved iteratively to update the transverse temperature profile. In all the cases investigated, a steady-state solution is reached after a sufficiently long integration period.

The number of calculation nodes is 61 in the z-direction and ranges between 61 (for $W = 1.0$ cm) and 121 (for $W = 6.0$ cm) in the y-direction. The calculation grids, both in the y and z directions, are considerably refined near the plate where the strongest velocity and temperature gradients occur. Test calculations have been carried out on finer grids in order to assess the influence of the grid size on the numerical results. Fig. 5 presents two instances of such test calculations for a copper plate with $W = 6.0$ cm at $Ra = 1.1 \times 10^5$ and a steel plate with $W = 5.0$ cm at $Ra = 5.8 \times 10^4$. Results in Fig. 5a have been obtained with the standard grid of 61 nodes along the z-direction, corresponding to a minimum spacing of $\Delta_z = 2.5 \times 10^{-4}$ m. Four different grids have been tested for the y-direction. The coarsest of these y-grids has a minimum spacing equal to $\Delta_y = 4.0 \times 10^{-3}$ m. In the three finer y-grids, the value of Δ_y is successively halved by doubling the number of y-calculation nodes. The dependence of the predicted Nu values on the grid spacing is very similar for the copper and the steel plates. Results in Fig. 5a for the coarsest y-grid are about 3% below the reference value, Nu_0, obtained from extrapolation to the $\Delta_y \to 0$ limit. The three finer grids yield heat transfer predictions in much closer agreement with the reference value in Fig. 5a. The value of $\Delta_y = 1.0 \times 10^{-3}$ m is chosen for the standard y-grid in a good balance between accuracy and economy. This choice of Δ_y results in a grid with 121 nodes along the y-direction for plates with $W = 6.0$ cm.

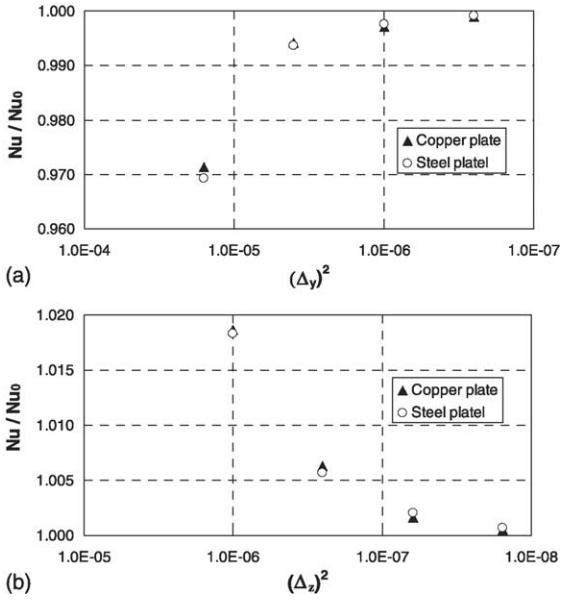

Fig. 5. Assessment of the influence of the grid spacing along the y (a) and z (b) directions on predicted Nusselt numbers in two-dimensional calculations. Results in this figure correspond to a copper plate of $W = 6.0$ cm at $Ra = 105{,}000$ and a steel plate of $W = 5.0$ at $Ra = 58{,}000$. The Nu_0 symbol stands for values of the Nusselt number that are extrapolated from the numerical predictions into the limit of zero grid spacing.

The Nu values shown in Fig. 5b have been obtained with the standard y-grid of $\Delta_y = 1.0 \times 10^{-3}$ m and four different z-grids. The largest value of the minimum grid spacing is $\Delta_z = 1.0 \times 10^{-3}$ m in this case, corresponding to a z-grid with only 16 nodes. This value of Δ_z is again successively halved in the three finer grids by doubling the number of nodes. The coarsest z-grid yields results that are almost 2% above the reference Nu_0 value in Fig. 5b. The finer z-grids yield considerably better predictions and the results in Fig. 5b suggest $\Delta_z = 2.5 \times 10^{-4}$ m as a proper choice for the standard z-grid. The conditions of W and Ra in the calculations of Fig. 5 have been chosen as most representative of the heat transfer results presented in Section 4.2 below. However, some of the results presented in there correspond to Rayleigh numbers as high as $Ra = 2 \times 10^6$. For these most exigent calculations, it has been found that the standard grids yield in the worst case predictions of Nu that differ in less than 3% from the corresponding results obtained on the finest grids.

In addition to the 2D calculations, several 3D calculations have also been performed using commercial software (FLUENT). Such 3D calculations are used at a qualitative level to visualize the 3D-flow structure in plates of a finite length and thus to complement the simplified picture of the flow structure given by 2D calculations.

4. Results and discussion

Experiments are carried out for the copper and steel plates listed in Table 1. The range of Rayleigh numbers covered is $290 \leqslant Ra_w \leqslant 3.3 \times 10^5$. Every plate is operated at several values of the electrical intensity, I, provided by the source. Measurements obtained from a given plate are then repeated two more times, normally at different days, for the same intensity values. The plates can be operated properly only within a certain range of the temperature drop, ΔT, which in most cases falls within the range $3.0 \leqslant \Delta T \leqslant 20$ K. Results are not satisfactorily reproduced for too low ΔT because of the uncertainty in the measurement of temperatures using either thermocouples or TLC's. As mentioned above, it is not possible to maintain the longitudinal isothermicity of the plate when it is operated at too high values of ΔT. The experimental procedure thus results in a limited range of Rayleigh numbers associated to each plate width. Note however that the widths of the plates listed in Table 1

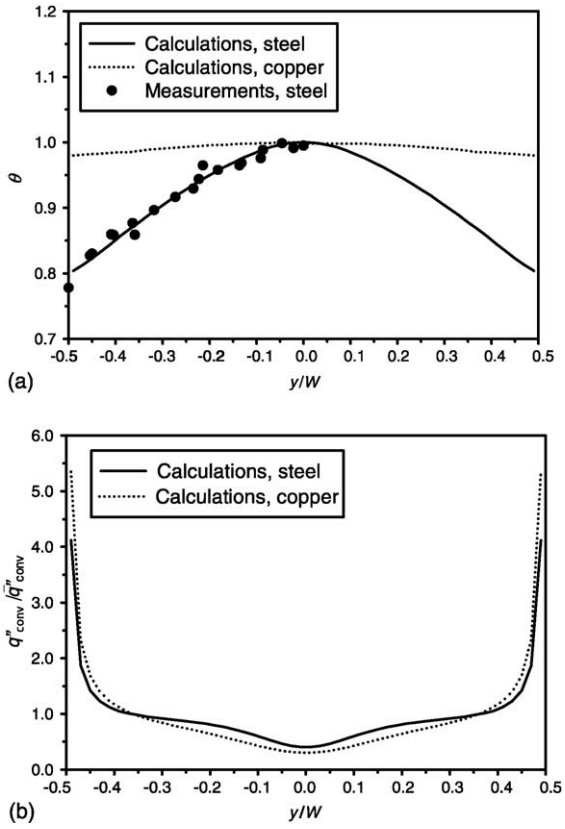

Fig. 6. Transverse profiles of several properties at the surface of a copper and a steel plate. Measured and calculated temperature profiles are compared in (a). The corresponding predictions of the local heat fluxes are shown in (b). Both measurements and predictions have been obtained for plates of width $W = 4.0$ cm.

guarantee that a broad range of Ra_w is covered on the overall. Calculations have been performed in the range of Rayleigh numbers with $1.1 \times 10^3 \leqslant Ra_w \leqslant 1.6 \times 10^6$ for copper and steel plates of widths $W = 1.0$, 2.5, 4.0, and 6.0 cm.

4.1. Flow structure and surface profiles

Two-dimensional calculations allow visualizing the structure of the flow and provide, thanks to the use of the boundary condition of Eq. (20), distributions of the temperature and the heat flux at the plate surface. Fig. 6a shows predicted and measured transverse profiles of temperature for a copper and a steel plate of width $W = 4.0$ cm. The corresponding transverse profiles of the surface heat flux are shown in Fig. 6b. The structure of the 2D flow in the region surrounding the plates is shown in Fig. 7a and b for the copper and the steel plate, respectively.

Calculations and measurements in Fig. 6a show important transverse variations of temperature at the surface of the steel plate, as is also reported by Sparrow and Carlson [12]. There is a good agreement between the measured and the predicted temperature profile. The increase of the surface temperature along the y-direction in Fig. 6a is accompanied, as shown in Fig. 7b, by the

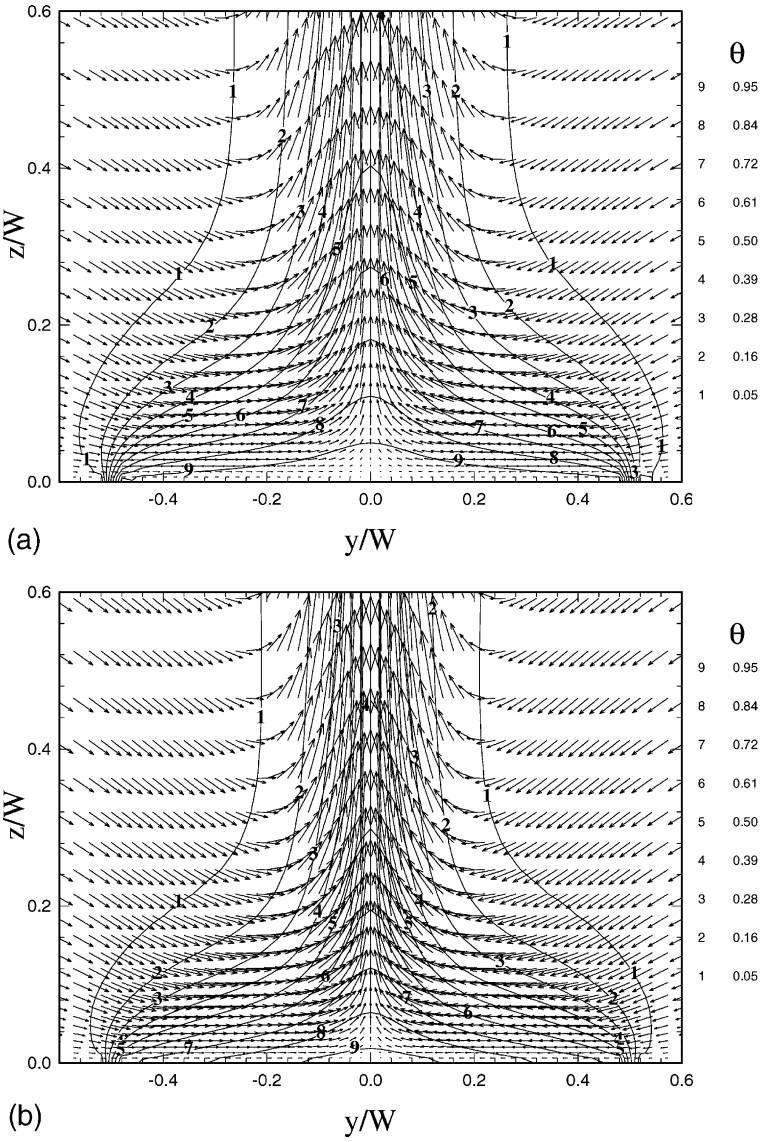

Fig. 7. Structure of the flow and temperature distribution of the air in the vicinity of the (a) copper and (b) steel plate for the same 2D calculations as in Fig. 6 above.

warming of the air traveling inwards near the surface of the plate. The flow structure and temperature contours shown in Fig. 7b are not very different from the corresponding ones for the copper plate, shown in Fig. 7a. However, the temperature profile at the surface of the copper plate is much flatter in Fig. 6a than it is for the steel plate. Such a difference is explained in terms of the transverse conduction of heat within the metal, represented by the last term in the RHS of Eq. (20). Because of the high thermal conductivity of copper, a significant amount of heat is being conducted from the center toward the edges of the plate.

The transverse variations of the local heat flux, shown in Fig. 6b, are very pronounced for both plates. Heat is transferred very efficiently from the surface near the edges of the plate where the air is still cold. The efficiency of the heat transfer from the surface decreases rapidly as the air travels inwards and it becomes progressively warmer (see Fig. 7). The local heat fluxes in Fig. 6b reach their minimum value at the center of the plate where warm air raises forming a plume. Note in Fig. 6b that the heat flux profile for the steel plate is essentially flat within a relatively wide region of the y-domain between the edge and the center of the plate. It seems therefore reasonable to compare, following Sparrow and Carlson [12], results for the steel plate with previous analyses for a uniform heat flux at the surface [18]. The corresponding profiles in Fig. 6a and b suggest that the surface distribution for copper plates be better approximated by the uniform temperature boundary condition.

Considering that such approximations to the two ideal surface conditions hold, calculated profiles of the local Nusselt number, Nu_y, are compared to the analyses of Pera and Gebhart [18] for a uniform temperature and a uniform heat flux in Fig. 8a and b, respectively. The analytical profiles have been obtained for a boundary layer that grows undisturbed along the y-direction. However, the calculated flows in Fig. 7a and b separate from the surface as they approach the center of the plate, thus quite a different physical situation. Near the center of the plate, the transfer of heat from the surface into the air is hindered by the flow separation that is observed in Fig. 7a and b.

On the other hand, three-dimensional calculations provide a more complete picture of the structure of the natural convection flow over a plate of finite length. Fig. 9 shows the streamlines computed in a 3D calculation for a plate with $W = 6.0$ cm and $L = 23.0$ cm. A uniform temperature distribution at the surface of the plate has been assumed for this particular calculation. Similar flow structures are also obtained from 3D calculations with a uniform heat flux at the surface and with a transverse temperature profile taken from measurements. The structure of the flow near the two plate ends is three-dimensional, but, on the overall, the flow suffers

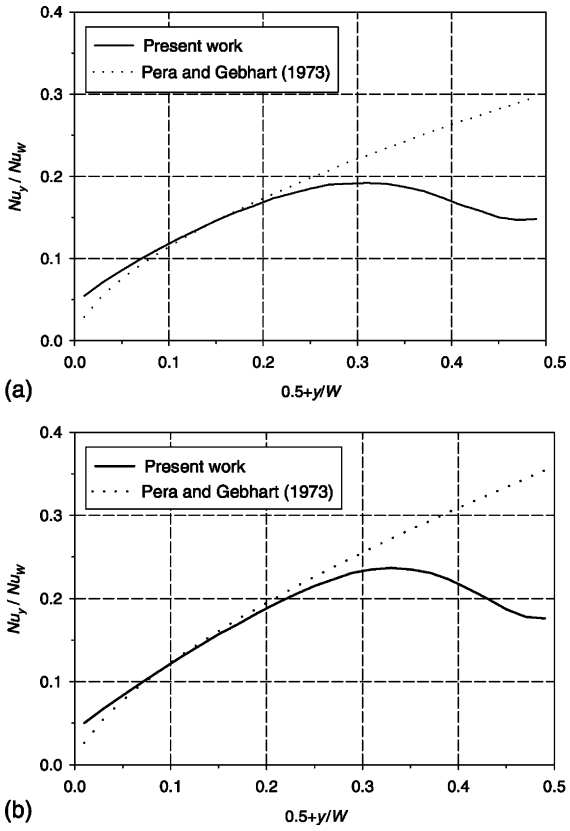

Fig. 8. Transverse profiles of the local Nusselt number, Nu_y, based on the distance from the edge of the plate. The calculated profile for a copper plate is compared in (a) with the boundary layer analysis [18] for the case with a uniform surface temperature. The calculated profile for a steel plate is compared in (b) with the boundary layer analysis for the case with a uniform surface flux [18]. Calculations correspond to the same conditions as in Figs. 6 and 7 above.

no dramatic change with respect to the 2D structure of Fig. 7a. As is shown in what follows, the three-dimensionality of the flow portrayed in Fig. 9 seems to have little effect on the overall heat transfer rates.

4.2. Average heat transfer coefficient

Present values of the heat transfer coefficient have been fitted, as discussed in Section 3.2 above, in the form of Eq. (14). Regression analyses with both $f(\phi) = \phi^m$ and $f(\phi) = \Gamma^m$ show that the present heat transfer data do not correlate with the aspect ratio of the plate. The values of the m exponent in the best fit are non-significant, e.g., their (absolute) value is small and the null hypothesis, $m = 0$, cannot be rejected. Moreover, the resulting equations fit data no better than does the correlation obtained by fixing $f(\phi) = 1$. Thus, the simpler form of Eq. (9) has been chosen to present the re-

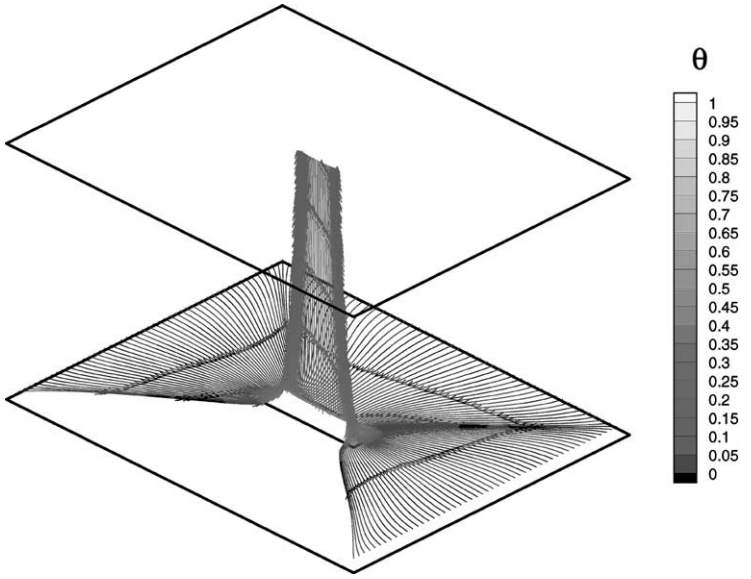

Fig. 9. Flow streamlines computed from a 3D calculation carried out with the Fluent software. The plate considered in the calculation is $W = 6.0$ cm wide and $L = 23.0$ cm long and its surface is assumed to be at a uniform temperature.

sults in Fig. 10a where numerical predictions are also included. The best fit to data in Fig. 10a is:

$$Nu_w = 1.23Ra_w^{0.173} \tag{21}$$

The best fit to experimental data alone yields similar values of $C = 1.20$ and $n = 0.175$. A very good fit with $C = 1.28$ and $n = 0.167$ is obtained from 2D calculations. Thus, there is a good agreement between the measured and the predicted heat transfer coefficients shown in Fig. 10a. It is noteworthy that despite of the different results for the copper and the steel plate in Figs. 6 and 7 above, no significant dependence on the type of metal is observed in Fig. 10a.

Since Eq. (21) does not account for a dependence of the Nusselt number on the aspect ratio, it appears to contradict the results reported by Lewandowski et al. [15]. It should be noted that present experiments and those of Lewandowski et al. share only the range of aspect ratios with $0.21 \leqslant \phi \leqslant 0.43$. Within this range, the geometry function proposed by Lewandowski et al., equivalent to $f(\phi) = \Gamma^{-0.40}$ in Eq. (14), varies in about 7%. This percentage of variation in Nu_w is lower than the relative width of the 95% prediction-interval for the fit of Eq. (21), which is about $\pm 11\%$. Thus, a dependence of Nu_w on the aspect ratio cannot be ruled out for the plates with the largest ratios investigated. Notwithstanding, it can be said that although the 3D flow pictured in Fig. 9 differs from the ideal 2D flow of Fig. 7 near the two plate ends, such a departure has little effect on the overall heat transfer rates. Far enough from the two ends, heat is transferred from the surface into the air as efficiently as it would be for a semi-infinite plate.

On the other hand, present measurements and calculations yield a value of $n \approx 0.17$ in Eq. (21) that is significantly below the theoretical exponent, $n = 1/5$. In this respect, it might be argued that the analyses in Ref. [18] are not fully applicable to the present problem, as suggested by Fig. 8. However, it must be recognized that the heat transfer data reported by Sparrow and Carlson [12] and Lewandowski et al. [15] are well fitted by the $n = 1/5$ exponent. The difference between present results and the measurements by these authors, who worked mainly in conditions such that $Ra_w \geqslant 10^6$, is to be attributed to the different range of Rayleigh numbers investigated. A low value of the n exponent is also predicted by Chambers and Lee [14], whose calculations yield $n = 0.138$ for $Ra_w \leqslant 1400$. A similar drop in the exponent with decreasing Rayleigh number has been reported for other natural convection flows. Examples are found in the measurements of McAdams [4] and Morgan [21] for long horizontal cylinders, and McAdams for vertical plates [4].

Such a behavior of the Ra_w^n term has to be related to the physics of the problem. At low Rayleigh numbers, the transverse diffusion of energy, represented in the RHS term of Eq. (19), is not negligible with respect to the convective transport terms. In the boundary layer equations, the transverse diffusion terms are however dropped [16,18,22]. It is consequently assumed that all of the heat transferred from the plate surface is transported along the y-direction by the fluid motion alone. When the Rayleigh number is low, the fluid motion is slow and the rate of heat transfer from the solid surface is constrained by the inability of the flow to convect

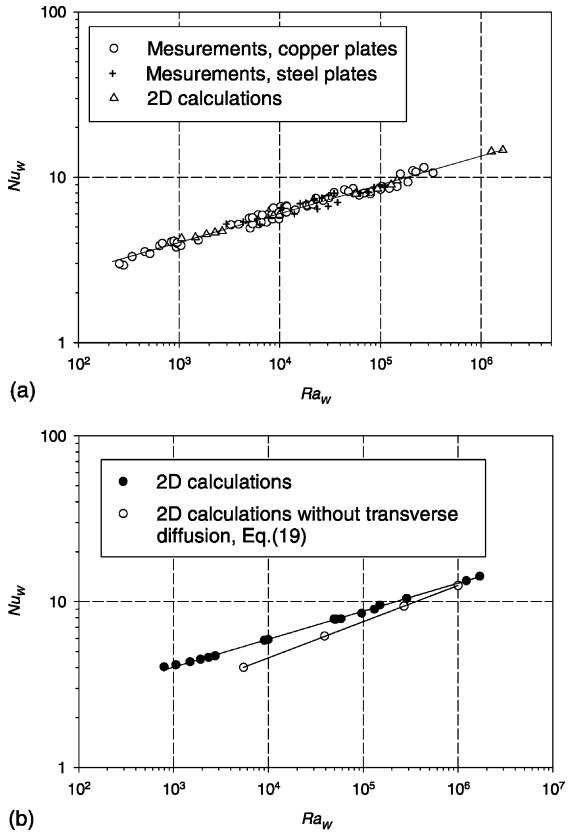

Fig. 10. Average heat transfer coefficients, cast in the form of Nu_w, are plotted as a function of the average Rayleigh number, Ra_w. Measurements and predictions are presented together in (a). Two-dimensional calculations are presented in (b). A second set of calculations is included in (b) where the transverse diffusion term in the energy equation (19) is neglected.

energy away. This is why boundary layer analyses yield the physically inconsistent limit of $Nu \to 0$ as $Ra \to 0$. In order to illustrate the effect of the transverse diffusion term in Eq. (19), a second set of 2D calculations has been carried out with this particular term artificially set to zero. Heat transfer predictions obtained from these altered calculations are compared in Fig. 10b with those obtained from the regular calculations, already included in Fig. 10a. The absence of the transverse diffusion term results in a significant variation of the heat transfer behavior as the parameters of the best fit change from $C = 1.28$ and $n = 0.167$ into $C = 0.616$ and $n = 0.218$.

In the real flow, diffusion along the y-direction is a feasible mechanism for removing heat away from the region above the plate. It follows that a purely conductive regime should be reached in the $Ra \to 0$ limit so that the Nusselt number should tend to a constant value as the Rayleigh number approaches zero. A common way to include low-Ra effects in heat transfer correlations for natural convection flows is the addition of a constant term to the RHS [23–26]. In this line, an alternative form to Eq. (9) is given by:

$$Nu_w = K + CRa_w^n \tag{22}$$

A different explanation is also found in the literature for the use of the K constant in Eq. (22). The similarity method, commonly used in boundary layer theory, suggests that the K constant symbolizes a shift in the y-origin with respect to the edge of the plate [27].

Since the influence of the y-diffusion term of Eq. (19) diminishes as the Rayleigh number increases, Eq. (22) would eventually tend to $Nu_w \approx CRa_w^n$, e.g., Eq. (9) above for sufficiently large values of Ra_w. Thus, heat transfer data that is compatible with previous analyses in [18] and measurements in [12,15] ought to be well fitted by Eq. (22) with $n = 1/5$. Present results meet this requirement, as shown in Fig. 11a where the difference $(Nu_w - K)$ is plotted against Ra_w. The corresponding plot for the 2D calculations alone is presented in Fig. 11b. By fixing the exponent to the theoretical value of $n = 1/5$, a good fit to data in Fig. 11a is given by $K = 0.78$ and $C = 0.820$. The corresponding fit to the numerical predictions in Fig. 11b yields $K = 1.12$ and

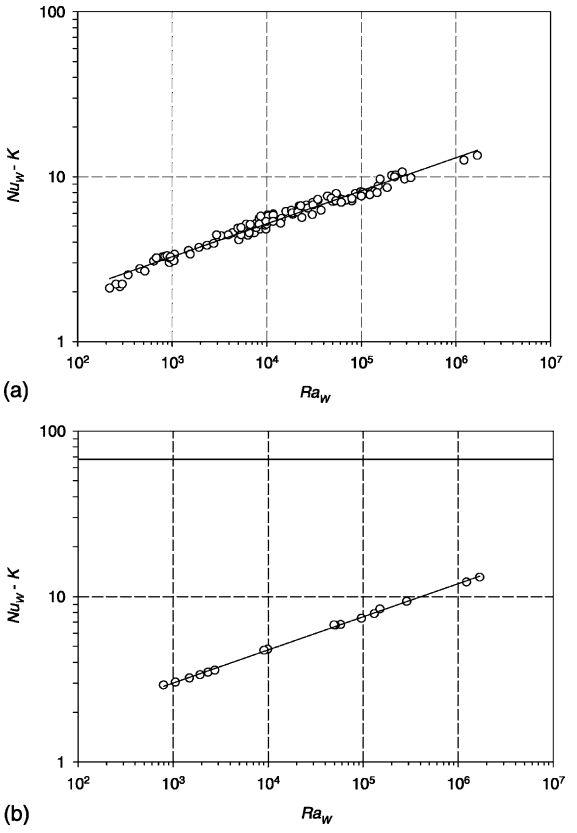

Fig. 11. The same heat transfer data as in Fig. 10 above is plotted in a form suitable to Eq. (22). The values of the K constant are $K = 0.78$ and (a) and $K = 1.12$ in (b).

$C = 0.754$. Since the fit with $n = 1/5$ to the data in Fig. 11a is almost as good as that of Eq. (21), it might be alternatively used to evaluate Nu_w within the range of parameters investigated in the present work.

Moreover, the above fits with the $n = 1/5$ exponent can be compared with the corresponding theoretical expressions given in [18] if the K constant is dropped from Eq. (22). The present value of $C = 0.82$ compares well with the corresponding theoretical prediction of $C = 0.85$ for an isothermal surface [18]. The theoretical analysis with a uniform heat flux at the surface [18] yields a somewhat higher value of $C = 0.93$. As shown in Fig. 6 above, the real boundary condition at the plate surface does not correspond either to the uniform temperature or to the uniform heat flux ideal assumptions. In addition, it should be kept in mind that the present problem is physically different from the one that is treated in the boundary layer analyses. In this respect, Pera and Gebhart [18] themselves report discrepancies between their analytical results and their own measurements. The authors attribute such discrepancies mainly to the separation of the flow from the surface, forming a rising thermal plume.

5. Conclusions

Measurements and calculations have been performed for the natural convection flow and heat transfer from horizontal plates cooled from above. Thinking of a future application to the design of printed circuit boards, the values considered of the Rayleigh number and the aspect ratio of the plate are below those investigated in previous works. Calculations are used to predict the structure of the flow and the local distribution of properties at the surface of the plate. The main flow structure consists of two opposing inward flows from the edges that meet at the center of the plate where warm air raises forming a thermal plume. The flow separation near the center of the plate considerably hinders the ability of the flow to remove heat from the surface. The implementation of boundary conditions that are appropriate to the problem of interest, e.g., a uniform heat generation per unit volume within the plate, reveals that the surface is neither isothermal nor of a uniform flux. Notwithstanding, the surface temperature predicted for copper plates is, due to the high conductivity of the metal, close to a uniform distribution. Important transverse gradients of temperature are measured and predicted for the steel plates instead. Neither a uniform temperature nor a uniform heat flux is a good model for the conditions at the surface of the steel plates, although the latter is probably closer to reality. Away from the edges and the center of the plate, the heat flux from the surface of the steel plate is essentially uniform.

Present experiments reveal no significant dependence of the Nusselt number on the aspect ratio of the plate. This observation seems to differ from part of the prior work on the subject, probably because most of the present measurements are obtained from plates narrower than those previously used by other researchers. Thus, although the flow near the two ends of the plate is 3D, such a departure from two-dimensionality has no significant influence on the averaged heat transfer coefficient, at least for long plates.

On the other hand, the value of the exponent in the present Nu–Ra fits, $n \approx 0.17$, is below the theoretical and most commonly accepted value of $n = 1/5$. However, the theoretical result is based on the boundary layer approximation, which precludes the possibility of removing heat just by conduction through the air. Thus, the theoretical dependence on $Ra_w^{1/5}$, even if it were actually applicable to the present problem, would be attained only at sufficiently high Rayleigh numbers. A more appropriate equation to correlate heat transfer data in the range of Rayleigh numbers investigated is therefore given by Eq. (22). When cast in this form, present heat transfer data do fit well to the analytical dependence on $Ra_w^{1/5}$ and the coefficient of the fit, C, is in a reasonable agreement with theory. Notwithstanding, comparisons between the present problem and that of an infinite boundary layer should be taken with caution. Boundary layer analyses do not predict any flow separation from the plate surface.

Acknowledgements

The present research has been mainly supported by the Spanish Government through the projects DGES-PB96-1011, DGESYIC-PPQ-2000-1339, and DGESYIC-DPI2000-1578-C02-01. Additional support has been received from the Catalan Government through projects 1998-SGR-00102, 1999-SGR-00338 and 2000-SGR-00103. These sources of funding are gratefully acknowledged.

References

[1] F.P. Incropera, Convection heat transfer in electronic equipment cooling, J. Heat Transfer 110 (1988) 1097–1111.
[2] J. Bigorra, F.J. Sánchez, I. Cuesta, J. Herrero, J. Giralt, F.X. Grau, ESTIMA: A thermal simulation software for the optimal design of printed circuit board in the automotive industry, in: Advanced Comp. Methods Heat Transfer, vol. VI, WIT Press, 2000, pp. 385–394.
[3] M. Fishenden, O.A. Saunders, An Introduction to Heat Transfer, Oxford University Press, 1950.
[4] W.H. McAdams, Heat Transmission, third ed., McGraw-Hill, 1954.

[5] K.E. Hassan, S.A. Mohamed, Natural convection from isothermal flat surfaces, Int. J. Heat Mass Transfer 13 (1970) 1873–1886.
[6] T. Fujii, H. Imura, Natural convection heat transfer from a plate with arbitrary inclination, Int. J. Heat Mass Transfer 15 (1972) 755–767.
[7] R.J. Goldstein, E.M. Sparrow, D.C. Jones, Natural convection mass transfer adjacent to horizontal plates, Int. J. Heat Mass Transfer 16 (1973) 1025–1035.
[8] J.R. Lloyd, W.R. Moran, Natural convection adjacent to horizontal surface of various platforms, J. Heat Transfer 96 (1974) 443–447.
[9] M. Al-Arabi, M.K. El-Riedy, Natural convection heat transfer from isothermal horizontal plates of different shapes, Int. J. Heat Mass Transfer 19 (1976) 1399–1404.
[10] R. Ishiguro, T. Abe, H. Nagase, Natural convection over heated horizontal plates, Trans. Jpn. Soc. Mech. Engrs., Ser. B 43 (1977) 638–645.
[11] W.W. Yousef, J.D. Tarasuk, W.J. McKenn, Free convection heat transfer from upward-facing isothermal horizontal surfaces, J. Heat Transfer 104 (1982) 493–500.
[12] E.M. Sparrow, C.K. Carlson, Local and average natural convection Nusselt numbers for a uniformly heated, shrouded or unshrouded horizontal plate, Int. J. Heat Mass Transfer 29 (1986) 369–379.
[13] K. Kitamura, F. Kimura, Heat transfer and fluid flow of natural convection adjacent to upward-facing horizontal plates, Int. J. Heat Mass Transfer 38 (1995) 3149–3159.
[14] B. Chambers, T.-Y.T. Lee, A numerical study of local and average natural convection Nusselt numbers for simultaneous convection above and below a uniformly heated horizontal thin plate, J. Heat Transfer 119 (1997) 102–108.
[15] W.M. Lewandowski, E. Radziemska, M. Buzuk, H. Bieszk, Free convection heat transfer and fluid flow above horizontal rectangular plates, Appl. Energy 66 (2000) 177–197.
[16] Y. Jaluria, Natural Convection Heat and Mass Transfer, Pergamon Press, 1980.
[17] D.J. Farina, R.J. Moffat, A system for making temperature measurements using thermochromic liquid crystals, Report no. HMT-48, Thermosciences Division, Department of Mechanical Engineering, Stanford University, 1994.
[18] L. Pera, B. Gebhart, On the stability of natural convection boundary layer flow over horizontal and slightly inclined surfaces, Int. J. Heat Mass Transfer 16 (1973) 1147–1163.
[19] J.A.C. Humphrey, C.A. Schuler, D. Webster, Unsteady laminar flow between a pair of disks corotating in a fixed cylindrical enclosure, Phys. Fluids 7 (1995) 1225–1240.
[20] J. Herrero, F. Giralt, J.A.C. Humphrey, Non-isothermal laminar flow and heat transfer between disks corotating in a fixed enclosure, Int. J. Heat Mass Transfer 42 (1999) 3291–3306.
[21] V.T. Morgan, The overall convective heat transfer from smooth circular cylinders, Adv. Heat Transfer 11 (1975) 199–264.
[22] Z. Rotem, L. Claassen, Natural convection above unconfined horizontal surfaces, J. Fluid Mech. 38 (1969) 173–192.
[23] T. Yuge, Experiments in heat transfer from spheres including combined natural and forced convection, J. Heat Transfer C 82 (1960) 214.
[24] S.W. Churchill, H.H.S. Chu, Correlating equations for laminar and turbulent free convection from a vertical plate, Int. J. Heat Mass Transfer 18 (1975) 1323–1329.
[25] S.W. Churchill, H.H.S. Chu, Correlating equations for laminar and turbulent free convection from a horizontal cylinder, Int. J. Heat Mass Transfer 18 (1975) 1049.
[26] S.W. Churchill, Heat Exchanger Design Handbook, Taylor and Francis, 1986.
[27] L.C. Burmeister, Convective Heat Transfer, second ed., John Wiley & Sons, 1993.